

Expanded View Figures

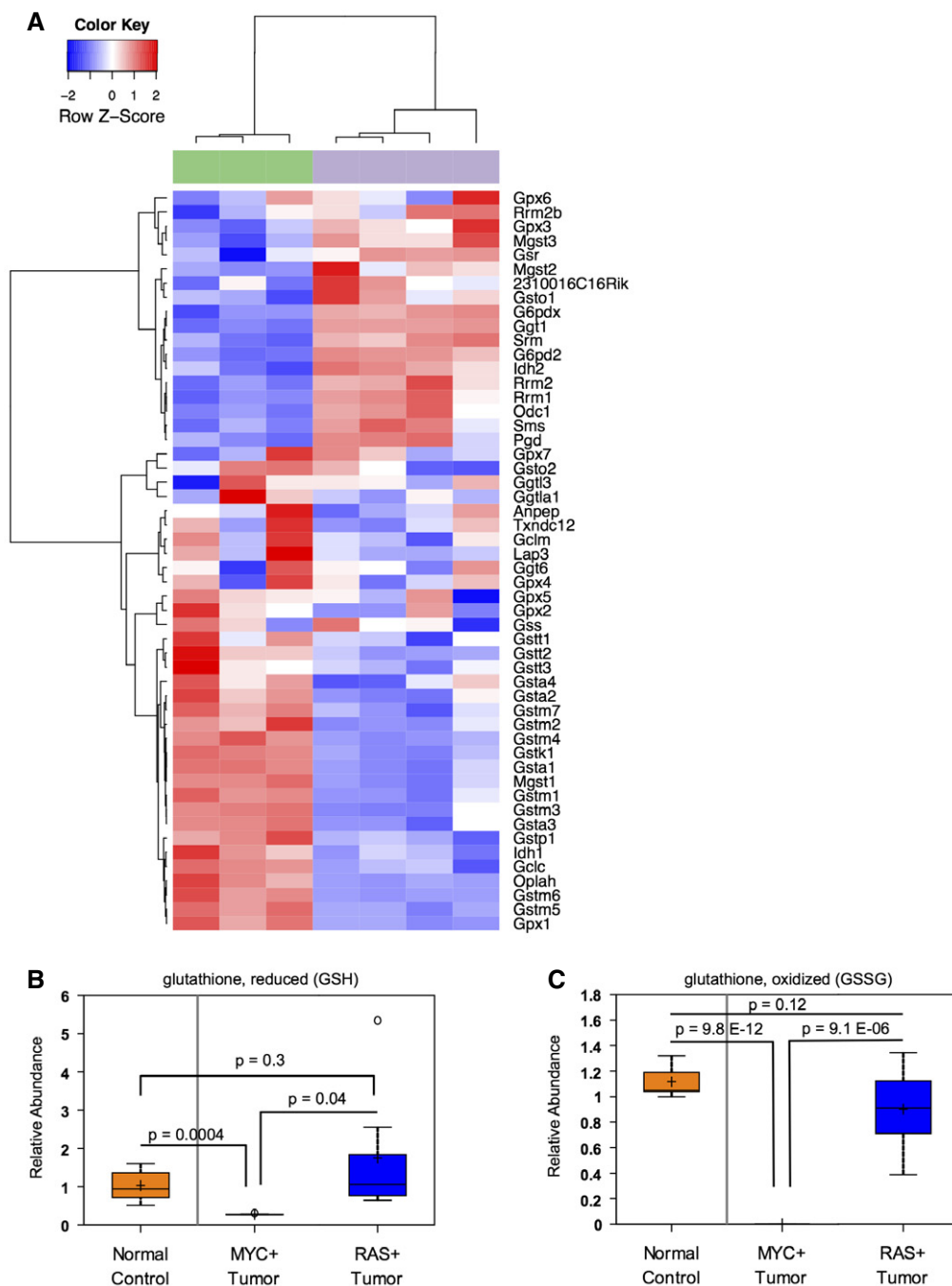


Figure EV1. Glutathione metabolism is altered in MYC-driven liver tumors.

- A Glutathione pathway transcript expression segregates LT2-MYC tumors from control livers by unsupervised hierarchical clustering ($n = 3$ control livers in green, $n = 4$ tumors in grey).
- B, C Relative metabolite abundance of GSH (B) or GSSG (C) in tissue samples from murine liver tumors driven by MYC or RAS, as compared to normal liver controls ($n = 7$ control liver, $n = 7$ MYC tumor, $n = 7$ RAS tumor, data represented as box plots with horizontal bar representing the median, box ranges representing the first (bottom) and third (top) quartiles, and vertical bars representing the standard error, unpaired two-tailed t -test, Bonferroni adjusted P -value for multiple comparisons is 0.02).

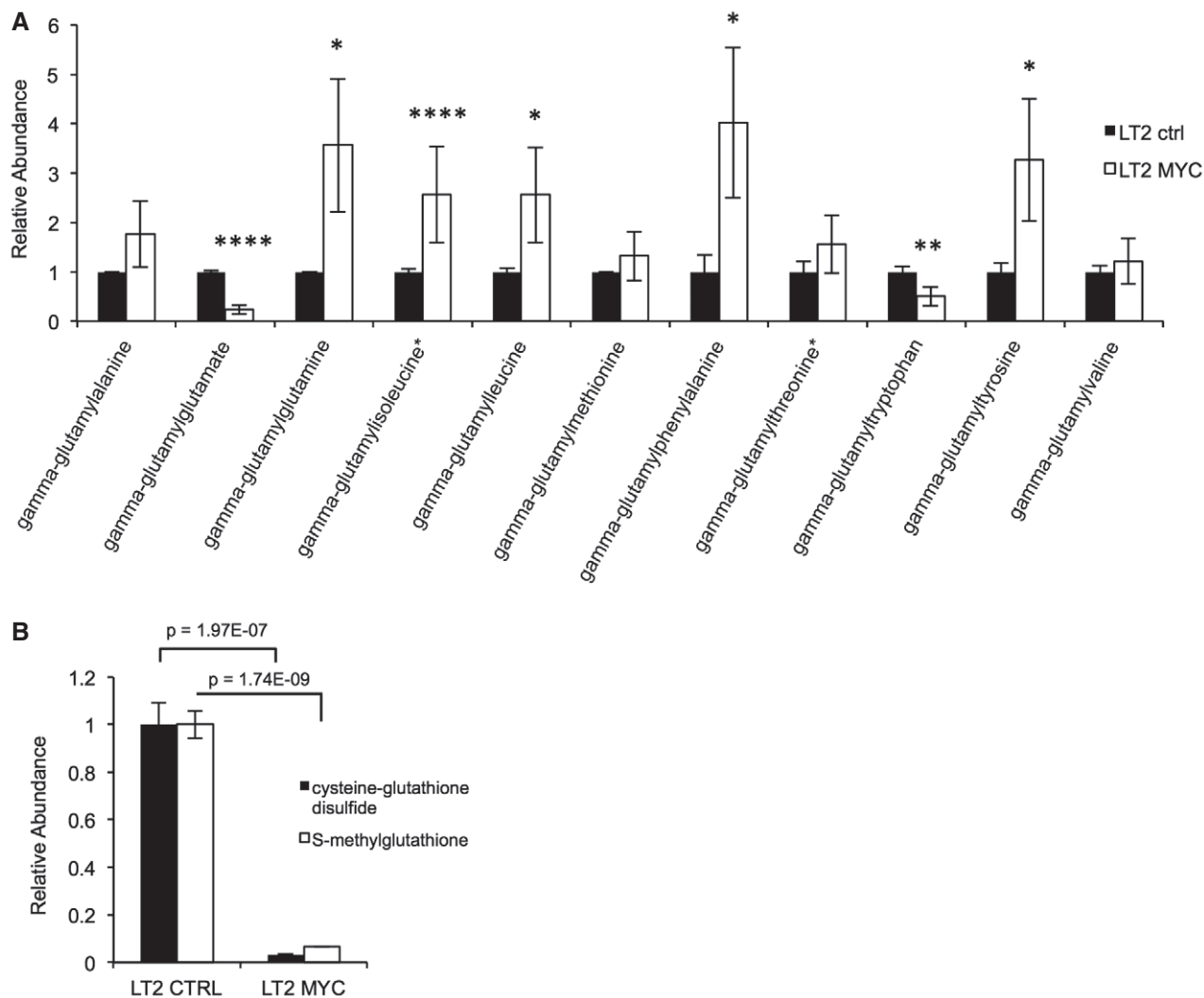


Figure EV2. Characterization of gamma-glutamyl amino acid and S-glutathylation abundance in MYC-driven liver tumors.

A Metabolite profiling of gamma-glutamyl amino acids in LT2-MYC tumors versus control livers ($n = 7$ control liver, $n = 7$ MYC tumor, data represented as normalized mean \pm SEM, unpaired two-tailed t -test, $*P < 0.05$, $**P < 0.01$, $****P < 0.00001$).

B Metabolite profiling of cysteine–glutathione disulfide and S-methylglutathione in LT2-MYC tumors versus control livers ($n = 7$ control liver, $n = 7$ MYC tumor, data represented as normalized mean \pm SEM, unpaired two-tailed t -test, cysteine–glutathione disulfide $P = 1.97305E-07$, S-methylglutathione $P = 1.73948E-09$).

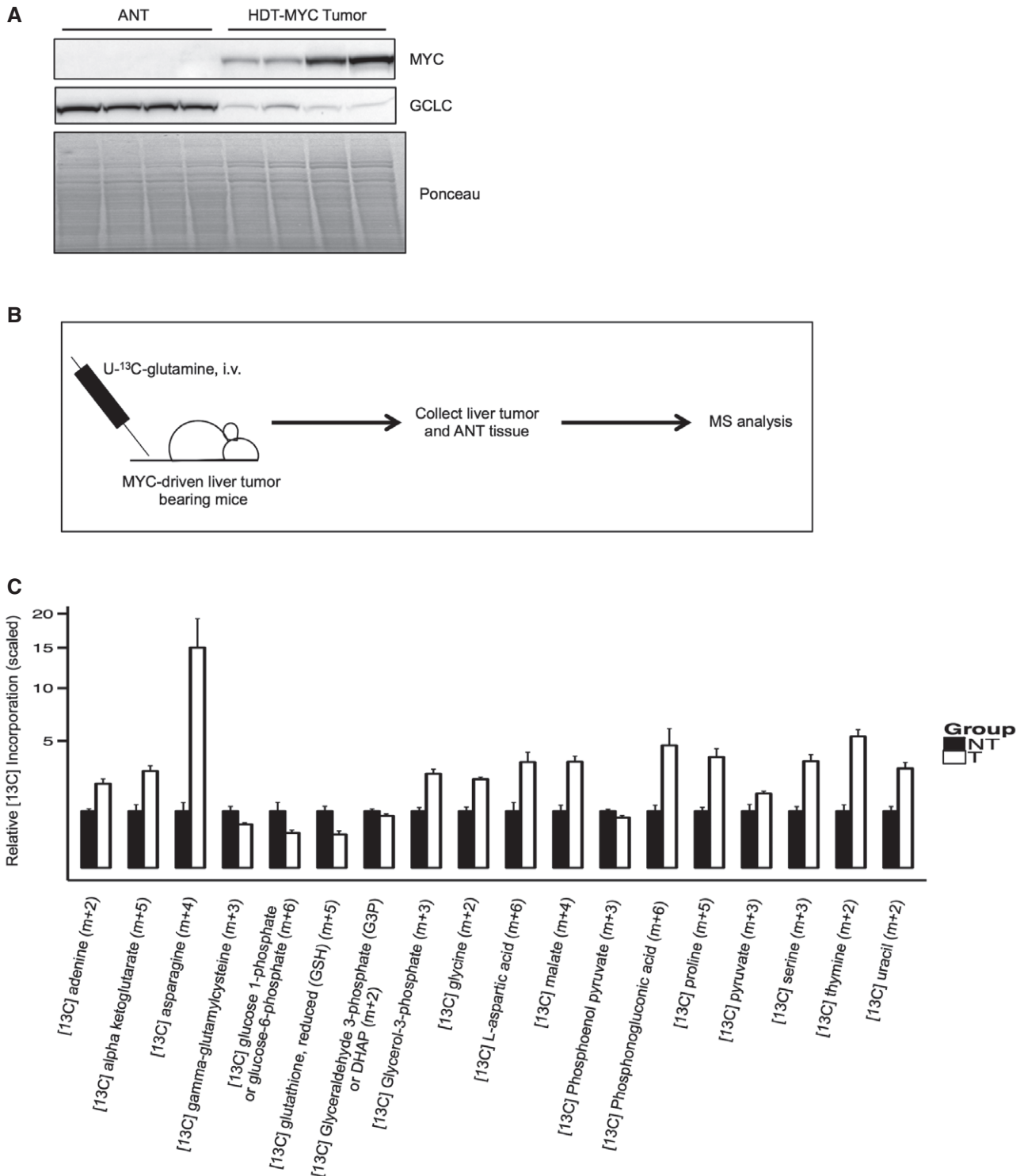


Figure EV3. Isotopic tracing of glutamine in MYC-driven liver tumors.

A Western blot analysis of MYC and GCLC protein expression in MYC-driven murine liver tumors established by hydrodynamic transfection [28] ($n = 4$ adjacent non-tumor (ANT), $n = 4$ MYC tumor).

B Schematic summary of U- ^{13}C -glutamine tracing experiment in MYC-driven liver tumor-bearing mice.

C Relative incorporation of U- ^{13}C -glutamine into metabolites in MYC-driven tumors compared to adjacent non-tumor liver tissue ($n = 6$ adjacent non-tumor (NT), $n = 6$ MYC tumor (T), all data represented as normalized mean \pm SEM, unpaired two-tailed t-test, all data significant at $P < 0.05$).

Source data are available online for this figure.

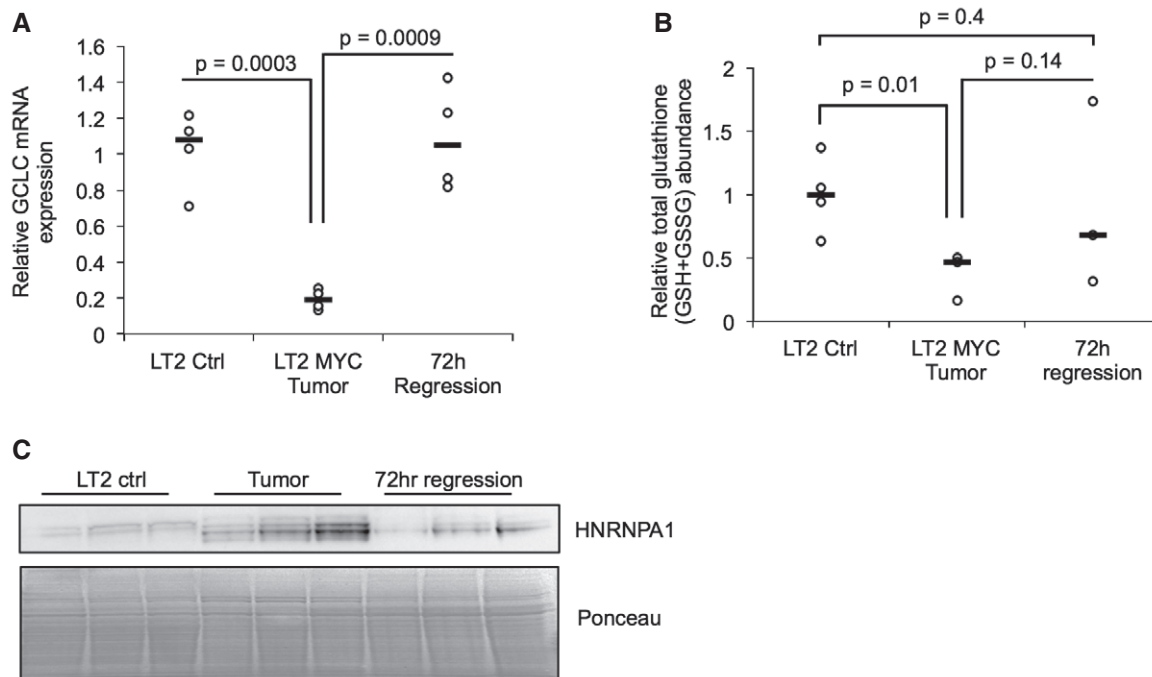


Figure EV4. GCLC expression and activity are altered in MYC-driven liver tumors.

A Quantitative PCR analysis of *Gclc* mRNA expression in LT2-MYC tumors, control livers, and liver tumors regressed for 72 h ($n = 4$ each group, data represented as univariate scatter plot with median, unpaired two-tailed t -test, LT2 ctrl versus LT2-MYC $P = 0.0003$, LT2-MYC versus 72 h regression $P = 0.0009$).

B Total glutathione (GSH + GSSG) abundance measured by enzymatic analysis in LT2 control livers, LT2-MYC tumors, and tumors regressed for 72 h ($n = 4$ LT2 ctrl, $n = 3$ LT2-MYC tumor, $n = 3$ 72 h reg tumor, data represented as univariate scatter plot with median, unpaired one-tailed t -test, LT2 ctrl versus LT2-MYC $P = 0.01$, LT2-MYC versus 72 h reg $P = 0.14$, LT2 ctrl versus 72 h reg $P = 0.4$, Bonferroni adjusted P -value is 0.02).

C Western blot analysis of HNRNPA1 in LT2-MYC tumors, control livers, and tumors regressed for 72 h ($n = 3$ each group).

Source data are available online for this figure.

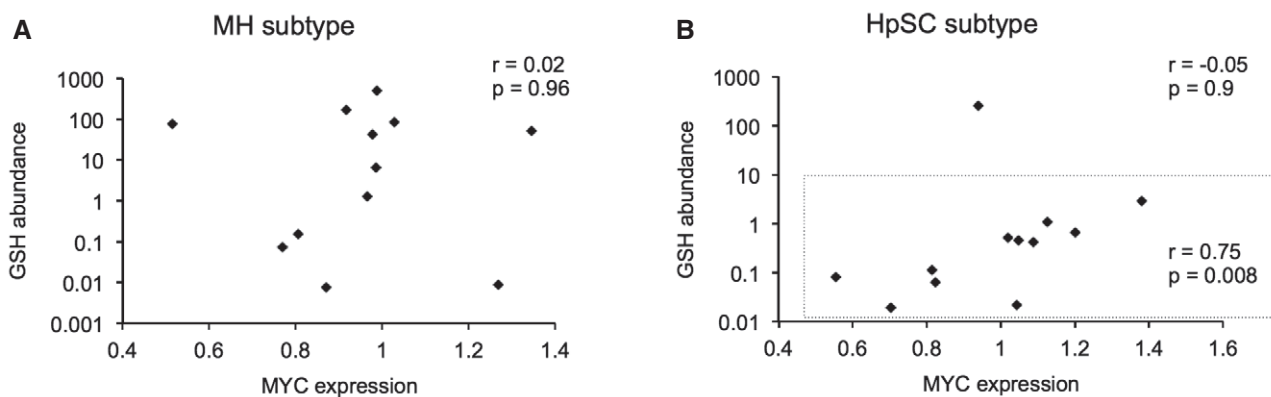


Figure EV5. Evaluation of relationship between GSH abundance and MYC expression in human liver cancer.

A, B Correlation plots of GSH abundance versus *MYC* mRNA expression in mature hepatocyte (MH) subtype (A) or hepatic stem cell (HpSC) subtype (B) of HCC tumors (samples from [40]) (MH: $n = 12$, Pearson coefficient = 0.02, two-tailed $P = 0.96$; HpSC: $n = 12$, Pearson coefficient = -0.05 , two-tailed $P = 0.9$; HpSC inset: $r = 0.75$ and two-tailed $P = 0.008$ when an outlier is removed).